Relativistic Topological and Spectral Characteristics of Zeolite SAS Structures

Micheal Arockiaraj[a,*], **Daniel Paul**[b], **Sandi Klavžar**[c,d,e], **Joseph Clement**[f], **Sushil Tigga**[a], **Krishnan Balasubramanian**[g]

[a]Department of Mathematics, Loyola College, Chennai 600034, India

[b]Department of Mathematics, Sri Sairam Institute of Technology, Chennai 600044, India

[c]Faculty of Mathematics and Physics, University of Ljubljana, Slovenia

[d]Faculty of Natural Sciences and Mathematics, University of Maribor, Slovenia

[e]Institute of Mathematics, Physics and Mechanics, Ljubljana, Slovenia

[f]Department of Mathematics, School of Advanced Sciences, Vellore Institute of Technology, Vellore 632014, India

[g]School of Molecular Sciences, Arizona State University, Tempe AZ 85287-1604, USA

Abstract

Zeolite SAS is a novel microporous zeotype material known as magnesioaluminophosphate with small pores and large cavities. The framework morphology of SAS is an excellent choice for isomorphic substitution to incorporate various types of metal ions into its pores, offering it distinct acidic and redox characteristics. Zeolite SAS type materials are receiving significant attention due to diverse applications in catalysis, iron exchange, environmental remediation and gas separation. A recent study shows that the SAS type materials remove, reduce or retard the adsorption of toxins, especially in water. In order to explore the structural characteristics of zeolite SAS and enhance its possible applications in QSPR and QSAR investigations, we employ graph theoretical techniques to derive the exact analytical formula of Wiener, Szeged, Mostar and degree type topological indices, which contain various information on molecules that can be useful in describing the physicochemical and biological properties of the materials. Furthermore we obtain the vertex partitions and spectral characteristics which in turn can aid in the interpretation of ESR and NMR spectral features as well as in relative comparisons of structures and their stabilities.

Keywords: Relativistic QSAR of materials; graph distance; partial cubes; zeolites.

*Corresponding author : marockiaraj@gmail.com

1 Introduction

Zeolites are crystalline inorganic polymers containing pores whose primary building blocks are MO_4 tetrahedra where M can be Si^{4+} or Al^{3+} cations or heteroatoms such as B, P, Sn, Ti, Fe, Ge, Ta, and V etc., are placed in the middle while the four oxygen atoms are at its corners [1, 2]. Every corner is connected with two MO_4 units that gives rise to a three dimensional structure comprising cavities of molecular size cross sections, channels and empty spaces which are known as micropores [3]. The openings of micropores, formed by rings of eight, ten, twelve, and more than twelve oxygen atoms, are categorized according to their pore size as small, medium, large, and extra-large zeolites respectively [5, 6]. The synthesis and catalysis of microporous molecules with such large cavities have gained considerable interest because of the various possible applications arising from their distinct properties and varied pore sizes [7,8]. The microporous zeolites have the unique capacity to incorporate various metal ions into its pores through the substitution of isovalent ions which give them distinct acidic and redox characteristics [4]. They have a number of unique properties due to their specific structures and electronic characteristics. Some of its distinctive properties include the existence of channels with well-defined dimensions, large amount of free space and lower density, higher degree of crystallinity, hydration, and the capacity of sorption of ions and molecules. The distinctive qualities of zeolites, such as structural specificity, large surface area, excellent thermal and chemical stability, and variable hydrophilic and hydrophobic characteristics, originate from their specific pore structures and molecular electronic structures [5]. These properties of zeolites have received the attention of researchers from various fields such as mineralogy, chemistry and industry [1]. Furthermore, the optimized zeotypes exhibit enhanced physicochemical characteristics such as excellent hydrothermal stability, fascinating gas separation ability, greater acidity and interesting catalytic properties [4]. The zeolite SAS is one such zeotype structure that exhibits such properties [9].

Zeolites also find applications in the domains of selective adsorption, catalysts, water softening and gas separation [10]. Zeolites are one of the most widely used materials in the chemical process industry and drug delivery [11]. The chemical composition of zeolites was initially limited to aluminosilicate polymorphs, but the ability to incorporate heteroatoms has given it new dimension of chemical versatility, allowing us to control the physicochemical properties of zeolites such as redox and acidic properties and its hydrophobic−hydrophilic nature, and thus the material finds a number of applications [5] including in luminescence, electricity, magnetism and microelectronic industries [12].

The microporous magnesioaluminophosphate which has the code SAS and the name St. Andrews-6 (STA-6) containing a one-dimensional channel system is a small pore zeolite SAS. It is obtained when MAPO (M = Mg, Mn, Fe, Co or Zn) or divalent metal cation-containing aluminophosphates

are hydrothermally synthesized by using the structure directing agent namely, azamacrocycle 1,4,8,11-tetramethyl-1,4,8,11-tetraazacyclotetradecane and introducing magnesium or other iron in the synthesis gel [13]. The unit cell of the zeolite SAS is composed of $Mg_3Al_{13}P_{16}O_{64}1.5R.2H_2O$. Zeolite SAS contains a one-dimensional channel system comprising of 8-membered rings. This system is composed of constricted cavities which are linked through common 8-membered rings. Figure 1 shows the building block of the SAS zeolite and the cavities that are linked by two 6-membered rings to form the zeolite SAS structure shown in Figure 2. The cages observed in zeolites A, RHO, and ZK-5 are slightly larger than the cages observed in zeolite SAS [14].

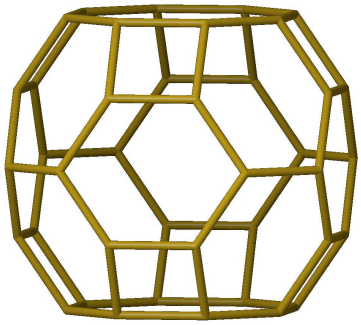

Figure 1: Building unit of zeolite SAS

In order to investigate the physicochemical properties of zeolite SAS material, we use chemical graph theory where the vertices represent the atoms and the edges denote the chemical bonds between them. Further we compute the topological indices of the SAS structures which have potential biological, chemical and physical applications through quantitative structure-activity relationship (QSAR) and quantitative structure-property relationship (QSPR) [15–19].

Relativistic effects including spin-orbit coupling are very important in the computation of electronic, structural and topological indices especially when very heavy atoms such as Au, Bi, Hg, Pt, Pd, etc., are present in the structure [20–22]. Therefore, it is very important to include relativistic parameters in the computation of topological indices of zeolite SAS materials. Both relativistic and nonrelativistic bond and charge parameters can be derived from high-level CASSCF/CI computations that can be carried out on such clusters, as demonstrated in the previous work on silicon clusters [23]. Thus, in the present manuscript, we compute topological indices for zeolite SAS materials which include relativistic effects. We use a relativistically weighted graph theoretical approach to derive exact mathematical formula of Wiener, Szeged, and Mostar type topological indices.

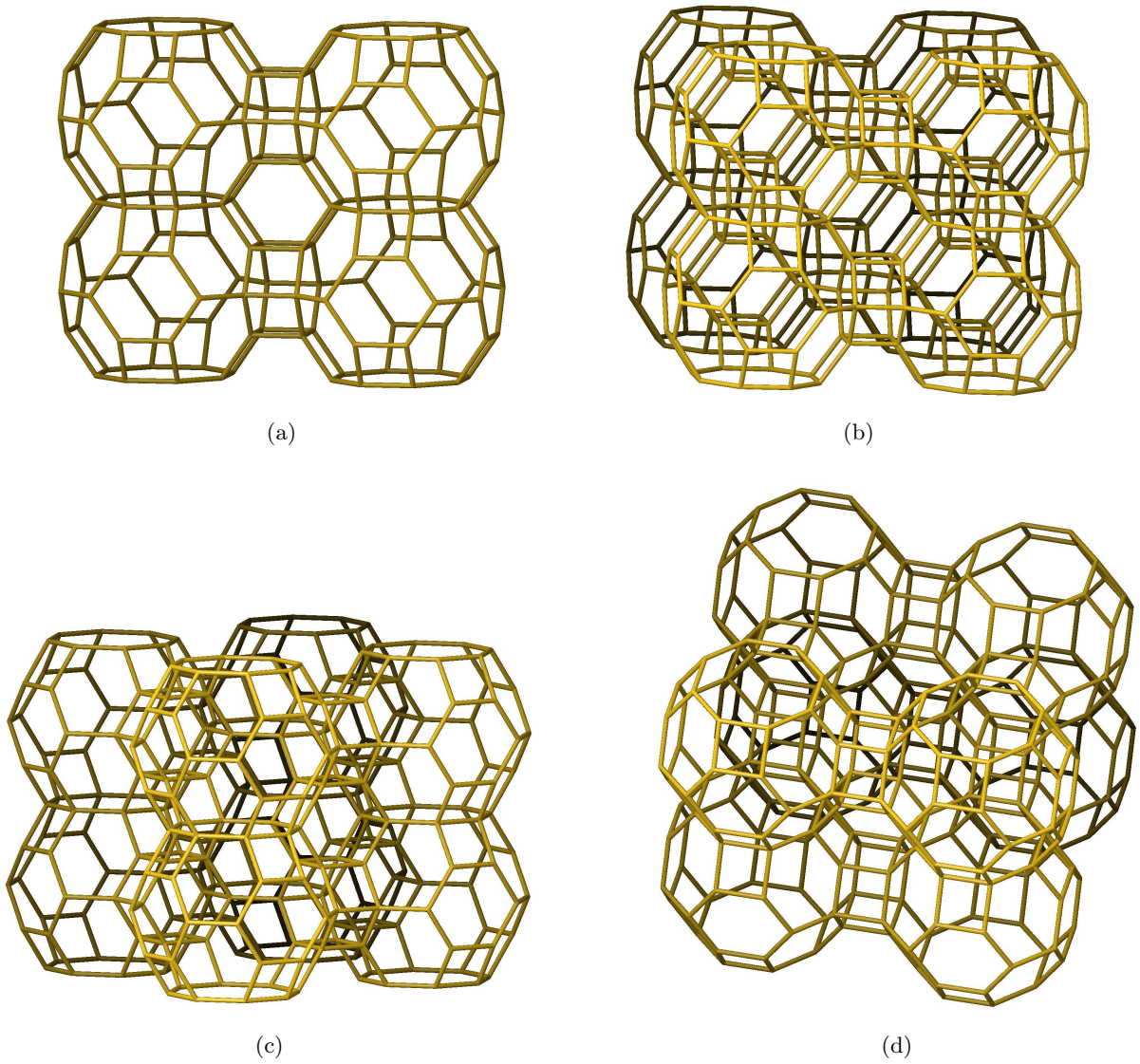

(a) (b) (c) (d)

Figure 2: (a) Square zeolite SAS of length 2 (b-d) Cubic zeolite SAS in front, side and top views

2 Partial Cubes and Topological Indices

A k-dimensional cube Q_k consists of a collection of k-bits binary strings in which two strings are connected by an edge if and only if the respective strings differ by exactly one bit. A collection of all isometric subgraphs (that is, distance preserving subgraphs) of all cubes Q_k, $k \geq 1$, is grouped into a family called partial cubes, which plays an essential part in the characterization of chemical properties of materials. We assume in this study that a partial cube graph Q_G has a vertex set $V(Q_G)$ consisting of all atoms, and an edge set $E(Q_G)$ consisting of bonds. The edge set of the partial cube graph Q_G can be partitioned into disjoint classes using the Djoković-Winkler relation Θ where two edges $e_j = x_j y_j$ and $e_k = x_k y_k$ are Θ related if $d_{Q_G}(x_j, x_k) + d_{Q_G}(y_j, y_k) \neq d_{Q_G}(x_j, y_k) + d_{Q_G}(x_k, y_j)$

in which $d_{Q_G}(x_j, x_k)$ stands for the distance between x_j and x_k.

It is a fundamental fact on partial cubes that Θ forms an equivalence relation on $E(Q_G)$. Let henceforth $\Theta(Q_G) = \{\Theta_1, \Theta_2, \ldots, \Theta_k\}$ be the Θ-based partition of the edge set of Q_G. The result of removing one Θ-class from Q_G, formally denoting this operation by $Q_G - \Theta_i$, is disconnected graph consisting of exactly two components [24–26]. Denoting the number of vertex elements and edge elements in one of these components by $n(\Theta_i)$ and $m(\Theta_i)$ respectively, then the number of vertex elements and edge elements in the other component will be denoted by $\overline{n}(\Theta_i)$ and $\overline{m}(\Theta_i)$. Clearly, $n(\Theta_i) + \overline{n}(\Theta_i) = |V(Q_G)|$ and $m(\Theta_i) + \overline{m}(\Theta_i) + |\Theta_i| = |E(Q_G)|$. For the topological indices of our interest the following expressions are known:

$$W(Q_G) = \sum_{i=1}^{k} n(\Theta_i)\overline{n}(\Theta_i) \quad \text{(Wiener index)}$$

$$W_e(Q_G) = \sum_{i=1}^{k} m(\Theta_i)\overline{m}(\Theta_i) \quad \text{(edge-Wiener index)}$$

$$W_{ev}(Q_G) = \sum_{i=1}^{k} \frac{1}{2}(n(\Theta_i)\overline{m}(\Theta_i) + \overline{n}(\Theta_i)m(\Theta_i)) \quad \text{(vertex-edge-Wiener index)}$$

$$Sz(Q_G) = \sum_{i=1}^{k} |\Theta_i| n(\Theta_i)\overline{n}(\Theta_i) \quad \text{(Szeged index)}$$

$$Sz_e(Q_G) = \sum_{i=1}^{k} |\Theta_i| m(\Theta_i)\overline{m}(\Theta_i) \quad \text{(edge-Szeged index)}$$

$$Sz_{ev}(Q_G) = \sum_{i=1}^{k} \frac{1}{2}|\Theta_i|(n(\Theta_i)\overline{m}(\Theta_i) + \overline{n}(\Theta_i)m(\Theta_i)) \quad \text{(edge-vertex-Szeged index)}$$

$$PI(Q_G) = |E(Q_G)|^2 - \sum_{i=1}^{k} |\Theta_i|^2 \quad \text{(Padmakar-Ivan index)}$$

$$S(Q_G) = \sum_{i=1}^{k} 2(n(\Theta_i)\overline{m}(\Theta_i) + \overline{n}(\Theta_i)m(\Theta_i)) + |E(Q_G)||V(Q_G)| \quad \text{(Schultz index)}$$

$$Gut(Q_G) = \sum_{i=1}^{k} (4m(\Theta_i)\overline{m}(\Theta_i) - |\Theta_i|^2) + 2|E(Q_G)|^2 \quad \text{(Gutman index)}$$

$$Mo(Q_G) = \sum_{i=1}^{k} |\Theta_i||n(\Theta_i) - \overline{n}(\Theta_i)| \quad \text{(Mostar index)}$$

$$Mo_e(Q_G) = \sum_{i=1}^{k} |\Theta_i||m(\Theta_i) - \overline{m}(\Theta_i)| \quad \text{(edge-Mostar index)}$$

The seminal of the above formulas, the one for the Wiener index, was proved in [24]. For later developments see the survey [25], and for the Szeged-like indices see the recent paper [27]; cf. also the references in the latter paper for other results.

The bond-type indices described above, such as Szeged index, Padmakar-Ivan index, and Mostar

index were strengthened in [28, 29] by including certain weights based on their end vertices degrees along with basic binary operations $\{+, *\}$ as described below. For $e_j = x_j y_j$, $w^+(e_j) = \deg_G(x_j) + \deg_G(y_j)$ and $w^*(e_j) = \deg_G(x_j)\deg_G(y_j)$, where $\deg_G(x_j)$ stands for the degree of vertex x_j. Further, set $w^+(\Theta_i) = \sum_{e_j \in \Theta_i} w^+(e_j)$, and $w^*(\Theta_i) = \sum_{e_j \in \Theta_i} w^*(e_j)$. If Q_G is a partial cube and $\circ \in \{+, *\}$, then the following formulas hold:

$$w^\circ Sz(Q_G) = \sum_{i=1}^{k} w^\circ(\Theta_i) n(\Theta_i) \overline{n}(\Theta_i) \quad \text{(weighted Szeged index)}$$

$$w^\circ Sz_e(Q_G) = \sum_{i=1}^{k} w^\circ(\Theta_i) m(\Theta_i) \overline{m}(\Theta_i) \quad \text{(weighted edge-Szeged index)}$$

$$w^\circ PI(Q_G) = \sum_{i=1}^{k} w^\circ(\Theta_i)(m(\Theta_i) + \overline{m}(\Theta_i)) \quad \text{(weighted Padmakar-Ivan index)}$$

$$w^\circ Mo(Q_G) = \sum_{i=1}^{k} w^\circ(\Theta_i)|n(\Theta_i) - \overline{n}(\Theta_i)| \quad \text{(weighted Mostar index)}$$

$$w^\circ Mo_e(Q_G) = \sum_{i=1}^{k} w^\circ(\Theta_i)|m(\Theta_i) - \overline{m}(\Theta_i)| \quad \text{(weighted edge-Mostar index)}$$

The Θ-based partition is not useful for computing the degree-based topological indices, whereas we consider another partition of the edge set of Q_G based on the bond end degrees [30–33]. Let D_{ij} be a set of bonds of Q_G such that $e_k = x_k y_k \in D_{ij}$, $\deg_G(x_k) = i$ and $\deg_G(y_k) = j$. We denote $D(Q_G) = \{D_{ij} : i \leq j, i, j \geq 1\}$ as the degree-based partition of Q_G. The corresponding degree-based indices ψ is defined by $\psi(Q_G) = \sum_{D_{ij} \in D(Q_G)} \psi(D_{ij})$ where $\psi(D_{ij}) = |D_{ij}|\psi(i, j)$ and the index function ψ for specific cases is given as follows: first Zagreb $M_1(i, j) = i + j$, second Zagreb $M_2(i, i) = ij$, Randić $R(i, j) = \frac{1}{\sqrt{ij}}$, atom-bond connectivity $ABC(i, j) = \sqrt{\frac{i+j-2}{ij}}$, harmonic $H(i, j) = \frac{2}{i+j}$, sum-connectivity $SC(i, j) = \frac{1}{\sqrt{i+j}}$, hyper-Zagreb $HM(i, j) = (i+j)^2$, geometric-arithmetic $GA(i, j) = \frac{2\sqrt{ij}}{i+j}$, irregularity $irr(i, j) = |i - j|$, forgotten $F(i, j) = i^2 + j^2$ and symmetric division degree $SDD(i, j) = \left(\frac{i}{j} + \frac{j}{i}\right)$.

There is a general method for calculating degree-based topological indices based on the M-polynomial: This polynomial was introduced in [34] as follows:

$$M(Q_G) = \sum_{i \leq j} |D_{ij}| x^i y^j .$$

It was then demonstrated in [34] that that degree-based topological indices can be routinely computed from the M-polynomial using derivation and integration. The method was afterwards used in more than a hundred papers, [35, 36] is just a sample couple of recent applications.

3 Results and Discussion

The basic building unit of zeolite SAS materials is composed of double 8-rings such that two consecutive connective bonds are replaced by (4,6,4)-rings and (6,6)-rings alternatively as shown in Figure 1 and that unit has 40 vertices and 60 edges. The key property needed for our investigation is that this building block is a partial cube. One way to verify this fact is be inspection, but this appears very tedious. However, this building block has been earlier discovered to be a partial cube in [37] by investigating the so-called tribes of partial cubes in order to discover as many cubic partial cubes as possible. Our current building block appeared in [37] as the graph B_{40}. The discovery of this graph was due to the investigation of the tribe of the truncated octahedron.

The building units are arranged horizontally and vertically, with horizontal units linked by double 6-rings and vertical units joined by 6-rings to form a rectangular zeolite SAS materials, as depicted in Figure 2a and denoted by $SAS(r, s)$. A cuboid form zeolite SAS material, denoted by $SAS(r, s, t)$, is an arrangement of $SAS(r, s)$ by t times such that the basic units in the two consecutive rectangular zeolite SAS materials are linked by double 6-rings. The above basic unit arrangement clearly shows that the number of vertices and edges of zeolite SAS materials as $|V(SAS(r, s, t))| = 8st(4r + 1)$ and $|E(SAS(r, s, t))| = 8st(8r + 1) - 6r(s + t)$, respectively and with reduction to $SAS(r, s)$ when $t = 1$.

The zeolite SAS materials are doped or impregnated with heavy atoms, and can be represented as weighted structural graph such that atoms and bonds weights are enabled by relativistic quantum parameters [17]. For this purpose, the weight γ_{x} is assigned to an atom x, and the weight ρ_{xy} is assigned to a bond x−y. In this study, we consider zeolite SAS materials with two heavy atoms x and y in an equal number by assigning vertex-weights $\{\gamma_{\mathrm{x}}, \gamma_{\mathrm{y}}\}$ and edge-weight ρ_{xy}. Let $V_\gamma(SAS(r, s, t))$ be the weighted vertex set of $SAS(r, s, t)$ such that $|V_\gamma(SAS(r, s, t))| = \frac{1}{2}\{\gamma_{\mathrm{x}} + \gamma_{\mathrm{y}}\}|V(SAS(r, s, t))|$. Similarly, let $E_\rho(SAS(r, s, t))$ be the weighted edge set of $SAS(r, s, t)$ such that $|E_\rho(SAS(r, s, t))| = \rho_{\mathrm{xy}}|E(SAS(r, s, t))|$.

The relativistic topological indices of rectangular and cuboid zeolite SAS materials are derived combining the Θ-classes of the basic units as viewed from the front, side and top with bond types such as forward, backward and vertical/horizontal as shown in Figure 3 and the Θ-classes denoted by FFV, FBV, FVV, SBV, SBV, SVV, TFV, and TBV. In addition, we use the bonds of double 6-rings to form the Θ-classes.

Theorem 3.1. *For $1 \leq r \leq s$, let $G = SAS(r, s)$. Then the following hold.*

(1) $W(G) = \frac{4}{15}(\gamma_{\mathrm{x}} + \gamma_{\mathrm{y}})^2[(960r^2 + 480r + 60)s^3 + (320r^3 + 480r^2 + 310r + 15)s^2 + (160r^4 + 160r^3 + 110r^2 - 40r - 15)s + (-32r^5 - 40r^4 - 10r^3 + 40r^2 + 42r)]$.

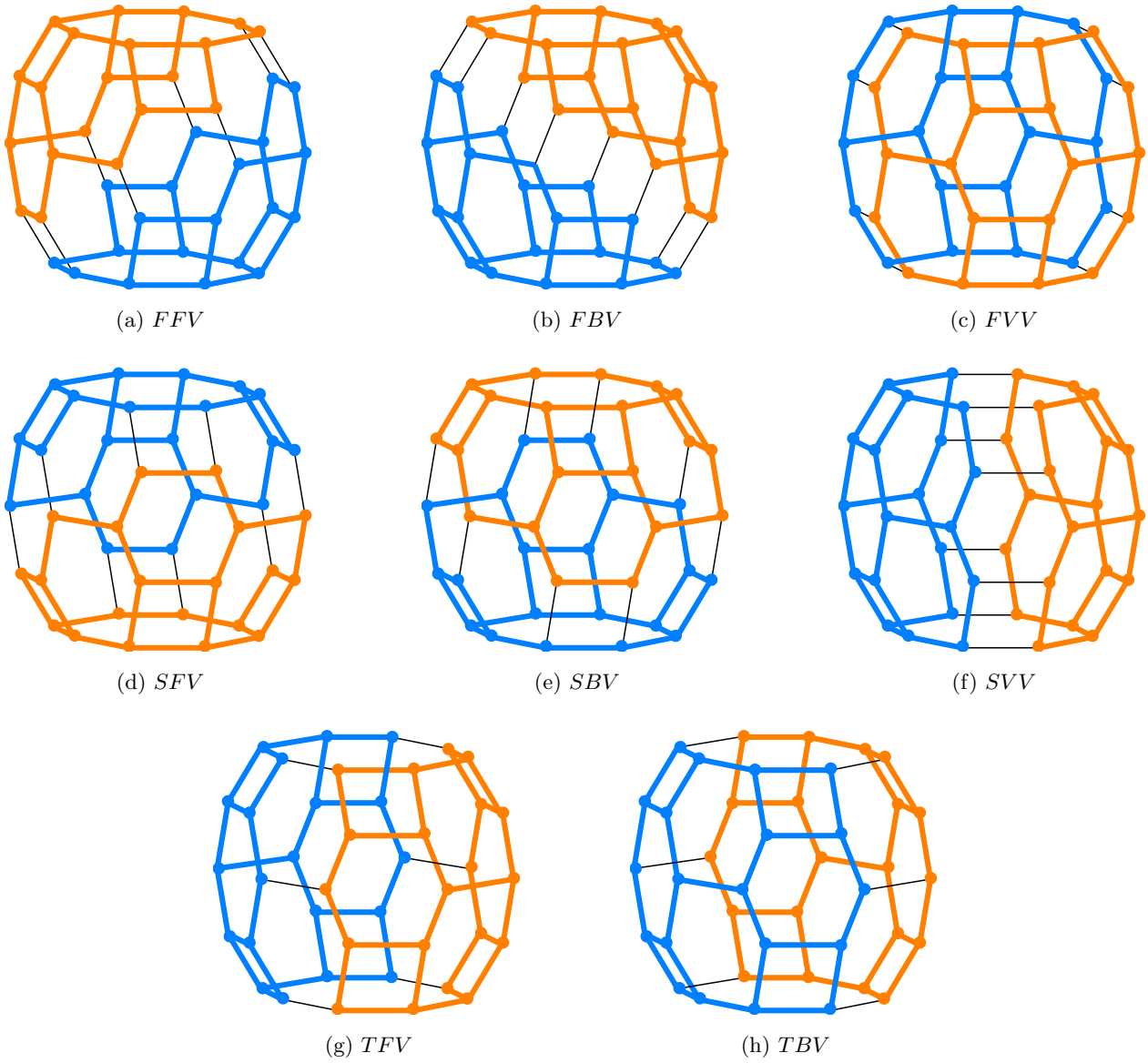

(a) FFV (b) FBV (c) FVV

(d) SFV (e) SBV (f) SVV

(g) TFV (h) TBV

Figure 3: (a-c) Front-view, (d-f) Side-view, (g-h) Top-view Θ-classes of the basic unit of zeolite SAS

(2) $W_e(G) = \frac{1}{15}\rho_{xy}^2[(50460r^2 + 13920r + 960)s^3 + (16820r^3 - 21180r^2 + 3820r - 225)s^2 + (8410r^4 + 1160r^3 + 10865r^2 - 1970r - 195)s + (-1682r^5 - 2030r^4 - 290r^3 + 1625r^2 + 2242r)]$.

(3) $W_{ev}(G) = \frac{2}{15}\rho_{xy}(\gamma_x + \gamma_y)[(4640r^2 + 1800r + 160)s^3 + (120r^2 + 90r + 15)s^2 + (1160r^4 + 900r^3 + 1100r^2 - 45r - 40)s + (-232r^5 - 285r^4 - 70r^3 + 285r^2 + 302r)]$.

(4) $Sz(G) = \frac{8}{15}\rho_{xy}(\gamma_x + \gamma_y)^2[(4880r^3 + 3480r^2 + 1345r + 45)s^3 + (160r^4 + 760r^3 + 440r^2 + 125r + 15)s + (-64r^5 - 340r^4 + 340r^2 + 64r)]$.

(5) $Sz_e(G) = \frac{2}{15}\rho_{xy}^3[(249080r^3+84150r^2+46225r+615)s^3+(-118380r^3-36600r^2-12600r-360)s^2+(20880r^4+68130r^3+6900r^2+2265r+285)s+(-3944r^5-19720r^4+1860r^3+19720r^2+464r)]$.

(6) $Sz_{ev}(G) = \frac{4}{15}\rho_{\rm xy}^2(\gamma_{\rm x}+\gamma_{\rm y})[(34840r^3+18330r^2+7415r+165)s^3+(-8220r^3-3735r^2-1050r-45)s^2+(2020r^4+6740r^3+2015r^2+415r+60)s+(-504r^5-2460r^4+240r^3+2460r^2+264r)]$.

(7) $PI(G) = \frac{4}{3}\rho_{\rm xy}^2[(2496r^2+582r+45)s^2+(-696r^2-114r-9)s+(32r^3+54r^2-32r)]$.

(8) $S(G) = \frac{8}{15}\rho_{\rm xy}(\gamma_{\rm x}+\gamma_{\rm y})[(6960r^2+2700r+240)s^3+(2320r^3+2010r^2+1685r+60)s^2+(1160r^4+660r^3+610r^2-345r-60)s+(-232r^5-285r^4-70r^3+285r^2+302r)]$.

(9) $Gut(G) = \frac{4}{15}\rho_{\rm xy}^2[(50460r^2+13920r+960)s^3+(16820r^3+3915r^2+10210r+240)s^2+(8410r^4+1160r^3+4775r^2-2900r-240)s+(-1682r^5-2030r^4-130r^3+2030r^2+2082r)]$.

(10) $Mo(G) = \frac{1}{3}\rho_{\rm xy}(\gamma_{\rm x}+\gamma_{\rm y})[(1248r^2+360r+192(-1)^r-156)s^2+(-288r^2-72r)s+(-32r^3-288r^2+96(-1)^s r^2-192(-1)^{r+s}r^2-112r+96(-1)^s r-48(-1)^{r+s}r+18(-1)^s-18)]$.

(11) $Mo_e(G) = \frac{1}{6}\rho_{\rm xy}^2[(9048r^2+1908r+1392(-1)^r-1248)s^2+(-2376r^2-288r-144(-1)^r+144)s+(-320r^3-2088r^2+696(-1)^s r^2-1392(-1)^{r+s}r^2-490r+618(-1)^s r-192(-1)^{r+s}r+72(-1)^s-72)]$.

(12) $w^+Mo(G) = \frac{2}{3}\rho_{\rm xy}(\gamma_{\rm x}+\gamma_{\rm y})[(4560r^2+780r+720(-1)^r-480)s^2+(-1632r^2-360r-96(-1)^r+96)s+(-80r^3-672r^2+312(-1)^s r^2-672(-1)^{r+s}r^2-190r+222(-1)^s r-120(-1)^{r+s}r+36(-1)^s+12(-1)^{r+s}-48)]$.

(13) $w^+Moe(G) = \rho_{\rm xy}^2[(11020r^2+1040r+1740(-1)^r-1212)s^2+(-4304r^2-432r-412(-1)^r+364)s+(-296r^3-1554r^2+754(-1)^s r^2-1624(-1)^{r+s}r^2-216r+452(-1)^s r-108(-1)^{r+s}r+24(-1)^s+40(-1)^{r+s}-88)]$.

(14) $w^*Mo(G) = 2\rho_{\rm xy}^2(\gamma_{\rm x}+\gamma_{\rm y})[(2800r^2+204r+448(-1)^r-276)s^2+(-1344r^2-216r-112(-1)^r+128)s+(-24r^3-248r^2+168(-1)^s r^2-400(-1)^{r+s}r^2-6r+66(-1)^s r-36(-1)^{r+s}r+6(-1)^s+16(-1)^{r+s}-22)]$.

(15) $w^*Mo_e(G) = \frac{1}{3}\rho_{\rm xy}^3[(60900r^2-204r+9744(-1)^r-5808)s^2+(-31248r^2-1536r-3444(-1)^r+3204)s+(-1072r^3-4626r^2+3654(-1)^s r^2-8700(-1)^{r+s}r^2+526r+1026(-1)^s r+192(-1)^{r+s}r+180(-1)^r+264(-1)^{r+s}-516)]$.

(16) $w^+Sz(G) = \frac{16}{15}\rho_{\rm xy}(\gamma_{\rm x}+\gamma_{\rm y})^2[(18080r^3+11360r^2+3040r+520)s^3+(-1120r^3-720r^2-410r)s^2+(400r^4+1820r^3+810r^2+295r+50)s+(-192r^5-1150r^4+250r^3+1270r^2+197r)]$.

(17) $w^+Sz_e(G) = \frac{4}{15}\rho_{\rm xy}^3[(920630r^3+232800r^2+101670r+26140)s^3+(-484810r^3-98370r^2-43670r-5940)s^2+(64670r^4+223190r^3-5570r^2+6785r+1160)s+(-12122r^5-66990r^4+17780r^3+70320r^2-483r)]$.

(18) $w^+PI(G) = \frac{8}{3}\rho_{\rm xy}^2[(9201r^2+1218r+66)s^2+(-3396r^2-153r+6)s+(112r^3+303r^2-127r)]$.

(19) $w^*Sz(G) = \frac{16}{15}\rho_{\rm xy}^2(\gamma_{\rm x}+\gamma_{\rm y})^2[(33760r^3+18560r^2+2990r+1315)s^3+(-3920r^3-2520r^2-1435r)s^2+(360r^4+1930r^3+280r^2+335r+95)s+(-272r^5-1965r^4+760r^3+2325r^2+277r)]$.

(20) $w^*Sz_e(G) = \frac{4}{15}\rho_{\rm xy}^4[(1715110r^3+300330r^2+97120r+75025)s^3+(-982640r^3-117870r^2-80695r-16020)s^2+(96860r^4+378125r^3-59780r^2+11675r+2375)s+(-17922r^5-115130r^4+45185r^3+125120r^2-5663r)]$.

(21) $w^*PI(G) = \frac{8}{3}\rho_{\rm xy}^3[(17097r^2+765r-51)s^2+(-7737r^2+243r+87)s+(200r^3+738r^2-263r)]$.

Proof. Since the rectangular zeolite SAS material is a partial cube graph, we need to classify the Θ-partition of $SAS(r,s)$ as well as the graph theoretical parameters $|\Theta_i|$, $n(\Theta_i)$, $m(\Theta_i)$, $w^+(\Theta_i)$, and $w^*(\Theta_i)$ for each class Θ_i in order to apply the computational techniques/formulas from Section 2. Let FFV_i, $1 \leq i \leq r+s-1$, be the Θ-classes consisting of forward-type bonds from the North-West corner of the rectangular SAS in front-view. In this fashion, we consider the backward-type bonds from the South-West corner to form the Θ-classes FBV_i, $1 \leq i \leq r+s-1$. Consequently, the topological quantities arising from FFV_i and FBV_i are the same. Let FVV_1 be a Θ-class covering all the horizontal bonds from the front-view direction.

In the side-view, let SFV_i and SBV_i, $1 \leq i \leq r$, be the Θ-classes consisting of forward and backward types bonding from the top to bottom of the rectangular SAS. The topological quantities of forward and backward Θ-classes are the same due to their symmetry and we will not mention them every time they are used. Let SVV_i, $1 \leq i \leq s$, be the Θ-classes consisting of horizontal bonds of the rectangular SAS from left to right in side-view, and let SHV_i, $1 \leq i \leq s-1$, be the Θ-classes consisting of double 6-ring bonds of rectangular SAS from left to right. Similar to side-view, let TFV_i and TBV_i, $1 \leq i \leq s$, be the Θ-classes resulting from top-view. The above mentioned Θ-classes are illustrated in Figure 4. For convenience, we write the Θ-classes that arrive from front-, side- and top-view respectively as F-, S- and T-type.

As previously stated, for any Θ-class Θ_i, $n(\Theta_i)+\overline{n}(\Theta_i) = |V_\gamma(SAS(r,s))|$ and $m(\Theta_i)+\overline{m}(\Theta_i)+|\Theta_i| = |E_\rho(SAS(r,s))|$, where $|V_\gamma(SAS(r,s))| = 4s(4r+1)\{\gamma_{\rm x}+\gamma_{\rm y}\}$ and $|E_\rho(SAS(r,s))| = 2(29rs+4s-3r)\rho_{\rm xy}$.

The topological parameters of F-type classes are computed as follows.

$$|FFV_i| = \begin{cases} 8i\rho_{\rm xy} & : 1 \leq i \leq r-1 \\ 8r\rho_{\rm xy} & : r \leq i \leq s \\ |FFV_{r+s-i}| & : s+1 \leq i \leq r+s-1 \end{cases}$$

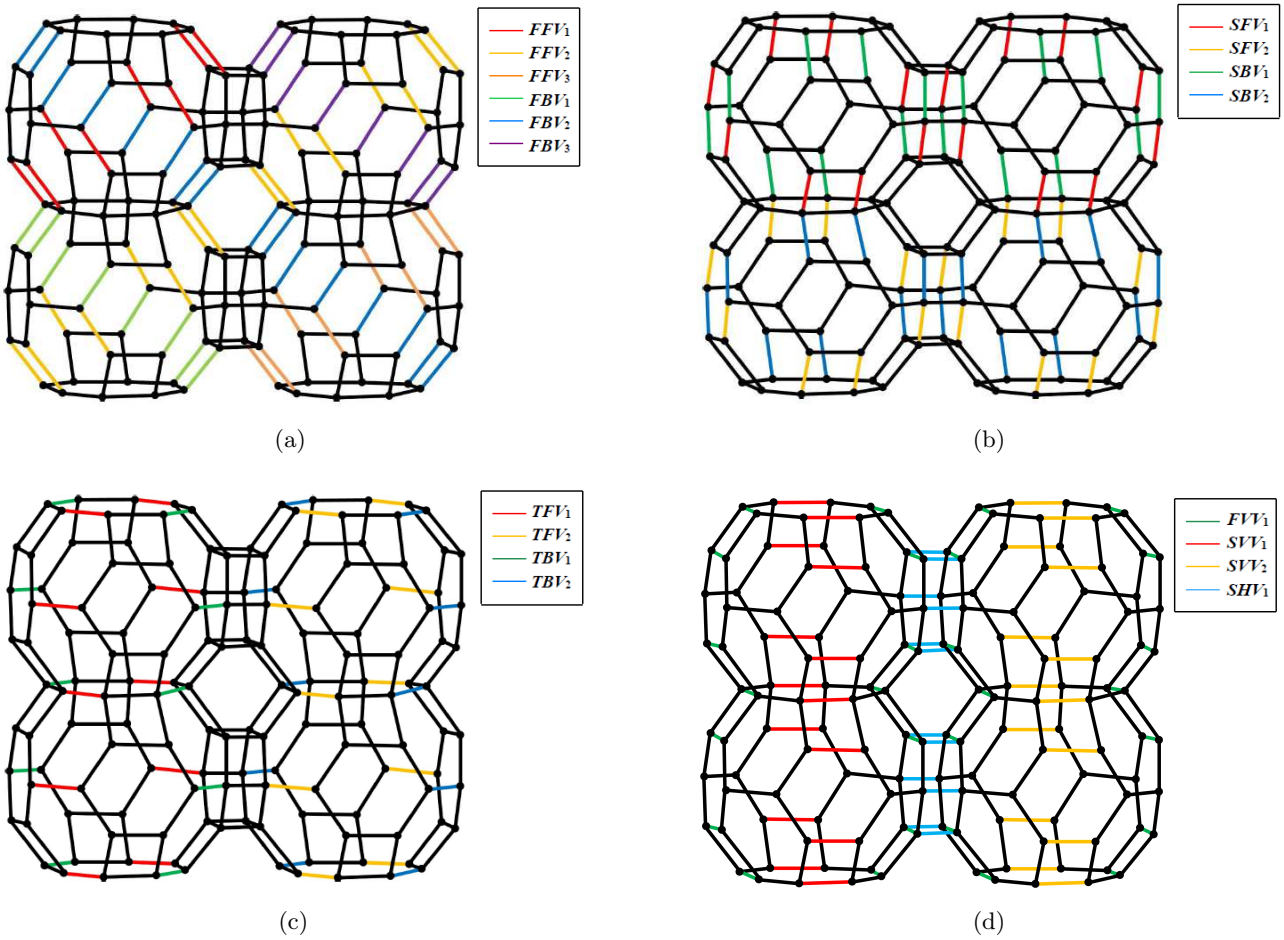

Figure 4: Θ-classes of $SAS(2,2)$

$$n(FFV_i) = \begin{cases} 2i(4i+1)\{\gamma_{\mathrm{x}} + \gamma_{\mathrm{y}}\} & : 1 \leq i \leq r-1 \\ 2(2i-r)(4r+1)\{\gamma_{\mathrm{x}} + \gamma_{\mathrm{y}}\} & : r \leq i \leq s \\ n(FFV_{r+s-i}) & : s+1 \leq i \leq r+s-1 \end{cases}$$

$$m(FFV_i) = \begin{cases} i(29i-3)\rho_{\mathrm{xy}} & : 1 \leq i \leq r-1 \\ (2i(29r+4) - r(29r+11))\rho_{\mathrm{xy}} & : r \leq i \leq s \\ m(FFV_{r+s-i}) & : s+1 \leq i \leq r+s-1 \end{cases}$$

$$w^{+}\left(FFV_{i}\right)=\begin{cases}4(14i-1)\rho_{\mathrm{xy}} & :\ 1\leq i\leq r-1\\ 8(7r-1)\rho_{\mathrm{xy}} & :\ i=r,\ r=s\\ 2(28r-3)\rho_{\mathrm{xy}} & :\ i=r,\ r<s\\ 4(14r-1)\rho_{\mathrm{xy}} & :\ r<i<s\\ w^{+}\left(FFV_{r+s-i}\right) & :\ s\leq i\leq r+s-1\end{cases}$$

$$w^{*}\left(FFV_{i}\right)=\begin{cases}4(25i-4)\rho_{\mathrm{xy}}^{2} & :\ 1\leq i\leq r-1\\ 4(25r-7)\rho_{\mathrm{xy}}^{2} & :\ i=r,\ r=s\\ 2(50r-11)\rho_{\mathrm{xy}}^{2} & :\ i=r,\ r<s\\ 4(25r-4)\rho_{\mathrm{xy}}^{2} & :\ r<i<s\\ w^{*}\left(FFV_{r+s-i}\right) & :\ s\leq i\leq r+s-1\end{cases}$$

$$\begin{aligned}\left|FVV_{1}\right|&=2s(3r+1)\rho_{\mathrm{xy}},\\ n\left(FVV_{1}\right)&=2s(4r+1)\{\gamma_{\mathrm{x}}+\gamma_{\mathrm{y}}\},\\ m\left(FVV_{1}\right)&=(26rs-3r+3s)\rho_{\mathrm{xy}},\\ w^{+}\left(FVV_{1}\right)&=8(6rs-(r-s))\rho_{\mathrm{xy}},\\ w^{*}\left(FVV_{1}\right)&=4(24rs-(7r-s))\rho_{\mathrm{xy}}^{2}.\end{aligned}$$

The topological parameters of S-type and T-type classes are given in the following.

$$\begin{aligned}\left|SFV_{i}\right|&=8s\rho_{\mathrm{xy}},\quad 1\leq i\leq r\\ n\left(SFV_{i}\right)&=2s(8i-3)\{\gamma_{\mathrm{x}}+\gamma_{\mathrm{y}}\},\quad 1\leq i\leq r\\ m\left(SFV_{i}\right)&=(29s-3)(2i-1)\rho_{\mathrm{xy}},\quad 1\leq i\leq r\end{aligned}$$

$$w^{+}\left(SFV_{i}\right)=\begin{cases}2(29s-4)\rho_{\mathrm{xy}} & :\ i\in\{1,r\}\\ 4(15s-2)\rho_{\mathrm{xy}} & :\ 1<i<r\end{cases}$$

$$w^{*}\left(SFV_{i}\right)=\begin{cases}2(53s-14)\rho_{\mathrm{xy}}^{2} & :\ i\in\{1,r\}\\ 28(4s-1)\rho_{\mathrm{xy}}^{2} & :\ 1<i<r\end{cases}$$

$$|SVV_i| = 2(3r+1)\rho_{\mathrm{xy}}, \quad 1 \le i \le s$$
$$n\,(SVV_i) = 2(4r+1)(2i-1)\{\gamma_{\mathrm{x}} + \gamma_{\mathrm{y}}\}, \quad 1 \le i \le s$$
$$m\,(SVV_i) = (2(29r+4)i - 5(7r+1))\rho_{\mathrm{xy}}, \quad 1 \le i \le s$$
$$w^{+}\,(SVV_i) = 8(5r+1)\rho_{\mathrm{xy}}, \quad 1 \le i \le s$$
$$w^{*}\,(SVV_i) = 4(17r+1)\rho_{\mathrm{xy}}^{2}, \quad 1 \le i \le s$$

$$|SHV_i| = 6r\rho_{\mathrm{xy}}, \quad 1 \le i \le s-1$$
$$n\,(SHV_i) = 4(4r+1)i\{\gamma_{\mathrm{x}} + \gamma_{\mathrm{y}}\}, \quad 1 \le i \le s-1$$
$$m\,(SHV_i) = 2((29r+4)i - 3r)\rho_{\mathrm{xy}}, \quad 1 \le i \le s-1$$

$$w^{+}\,(SHV_i) = 48r\rho_{\mathrm{xy}}, \quad 1 \le i \le s-1$$
$$w^{*}\,(SHV_i) = 96r\rho_{\mathrm{xy}}^{2}, \quad 1 \le i \le s-1$$

$$|TFV_i| = 2(2r+1)\rho_{\mathrm{xy}}, \quad 1 \le i \le s$$
$$n\,(TFV_i) = 2(4r+1)(2i-1)\{\gamma_{\mathrm{x}} + \gamma_{\mathrm{y}}\}, \quad 1 \le i \le s$$
$$m\,(TFV_i) = 2(29r+4)i - (34r+5)\rho_{\mathrm{xy}}, \quad 1 \le i \le s$$

$$w^{+}\,(TFV_i) = \begin{cases} (29r+8)\rho_{\mathrm{xy}} & : i \in \{1, s\} \\ 2(15r+4)\rho_{\mathrm{xy}} & : 1 < i < s \end{cases}$$

$$w^{*}\,(TFV_i) = \begin{cases} (53r+4)\rho_{\mathrm{xy}}^{2} & : i \in \{1, s\} \\ 4(14r+1)\rho_{\mathrm{xy}}^{2} & : 1 < i < s \end{cases}$$

The proof is complete when the topological parameters obtained from each class are added together using the following equation, where $\psi(\Theta)$ represents the topological parameters obtained by the cut method for the class Θ with respect to the topological index function ψ.

$$\psi(SAS(r,s)) = 4\sum_{i=1}^{r-1}\psi(FFV_i) + 2\sum_{i=r}^{s}\psi(FFV_i) + \psi(FVV_1) + 2\sum_{i=1}^{r}\psi(SBV_i) + \sum_{i=1}^{s}TI(SVV_i) + \sum_{i=1}^{s-1}\psi(SHV_i) + 2\sum_{i=1}^{s}\psi(TBV_i).$$

□

Theorem 3.2. *For $r \le s \le t$, let $G = SAS(r,s,t)$. Then the following hold.*

(1) $W(G) = \frac{4}{15}(\gamma_{\mathrm{x}} + \gamma_{\mathrm{y}})^2[(-32s^2 - 32t^2)r^5 + (160s^2t - 40s^2 + 160st^2 - 40t^2)r^4 + (160s^2t - 10s^2 + 160st^2 - 10t^2)r^3 + (-32s^5 + 160s^4t + 640s^3t^2 + 960s^2t^3 - 50s^2t + 40s^2 - 50st^2 + 32s + 40t^2)r^2 +$

$(-16s^5+80s^4t+320s^3t^2+480s^2t^3-120s^2t+42s^2-120st^2+16s+42t^2)r+(-2s^5+10s^4t+40s^3t^2+60s^2t^3-25s^2t-25st^2+2s)]$.

(2) $W_e(G)=\frac{1}{15}\rho_{\rm xy}^2[(-2048s^2+384s-2048t^2+384t-36)r^5+(10240s^2t-2240s^2+10240st^2-3840st+300s-2240t^2+300t)r^4+(5120s^2t-470s^2+5120st^2-960st-470t^2)r^3+(-2048s^5+10240s^4t+40960s^3t^2-11520s^3t+500s^3+61440s^2t^3-59520s^2t^2+7030s^2t+1700s^2-11520st^3+6910st^2+2760st+1653s+540t^3+1700t^2-435t)r^2+(-512s^5+2560s^4t+10240s^3t^2-1440s^3t-40s^3+15360s^2t^3-11280s^2t^2-2550s^2t+2518s^2-1440st^3-2670st^2+960st+168s+2518t^2-384t+36)r+(-32s^5+160s^4t+640s^3t^2-10s^3+960s^2t^3-480s^2t^2-355s^2t-385st^2+42s)]$.

(3) $W_{ev}(G)=\frac{2}{15}\rho_{\rm xy}(\gamma_{\rm x}+\gamma_{\rm y})[(-256s^2+24s-256t^2+24t)r^5+(1280s^2t-300s^2+1280st^2-240st+15s-300t^2+15t)r^4+(960s^2t-70s^2+960st^2-120st-70t^2)r^3+(-256s^5+1280s^4t+5120s^3t^2-720s^3t+7680s^2t^3-3720s^2t^2-160s^2t+300s^2-720st^3-160st^2+240st+241s+300t^2-15t)r^2+(-96s^5+480s^4t+192s^3t^2-180s^3t+2880s^2t^3-1170s^2t^2-630s^2t+326s^2-180st^3-630st^2+120st+72s+326t^2-24t)r+(-8s^5+40s^4t+160s^3t^2+240s^2t^3-60s^2t^2-100s^2t-100st^2+8s)]$.

(4) $Sz(G)=\frac{8}{15}\rho_{\rm xy}(\gamma_{\rm x}+\gamma_{\rm y})^2[(-64s^3-64t^3)r^5+(160s^3t-340s^3+160st^3-340t^3)r^4+(-160s^4+5120s^3t^3+760s^3t+160s^2+440st^3)r^3+(-160s^4+3200s^3t^3+440s^3t+340s^3+160s^2+120st^3+340t^3)r^2+(-50s^4+640s^3t^3+125s^3t+64s^3+50s^2+25st^3+64t^3)r+(-5s^4+40s^3t^3+15s^3t+5s^2+5st^3)]$.

(5) $Sz_e(G)=\frac{2}{15}\rho_{\rm xy}^3[(-4352s^3+408s^2-4352t^3+408t^2)r^5+(23040s^3t-23380s^3-2160s^2t+3840s^2+23040st^3-2160st^2-180s-23380t^3+3840t^2-180t)r^4+(-384s^5+4480s^4t-10600s^4+327680s^3t^3-134400s^3t^2+77700s^3t+4140s^3-122880s^2t^3+18360s^2t^2-14740s^2t+10240s^2+56500st^3-6420st^2+1050st-1536s+2220t^3-360t^2)r^3+(-240s^5+4080s^4t-8100s^4+122880s^3t^3-40800s^3t^2+8190s^3t+24580s^3-29760s^2t^3+2880s^2t^2-5880s^2t+4260s^2-8010st^3+600st^2+510st-780s+23380t^3-3840t^2+180t)r^2+(-24s^5+1080s^4t-1590s^4+15360s^3t^3-5880s^3t^2+2205s^3t+632s^3-2760s^2t^3+360s^2t^2-1440s^2t+1542s^2-975st^3-120st^2+60st-96s+512t^3-48t^2)r+(80s^4t-95s^4+640s^3t^3-360s^3t^2+285s^3t-120s^2t^3-80s^2t+95s^2+95st^3)]$.

(6) $Sz_{ev}(G)=\frac{4}{15}\rho_{\rm xy}^2(\gamma_{\rm x}+\gamma_{\rm y})[(-528s^3+24s^2-528t^3+24t^2)r^5+(2080s^3t-2700s^3-60s^2t+240s^2+2080st^3-60st^2-2700t^3+240t^2)r^4+(-24s^5+280s^4t-1280s^4+40960s^3t^3-8400s^3t^2+7280s^3t+360s^3-7680s^2t^3-820s^2t+1280s^2+4720st^3-300st^2-96s+240t^3)r^3+(-18s^5+290s^4t-1120s^4+20480s^3t^3-3600s^3t^2+2270s^3t+2790s^3-2820s^2t^3-545s^2t+880s^2+30st^3-75st^2-72s+2700t^3-240t^2)r^2+(-3s^5+95s^4t-280s^4+3200s^3t^3-555s^3t^2+460s^3t+303s^3-285s^2t^3-140s^2t+256s^2-100st^3-15st^2-12s+288t^3-24t^2)r+10s^4t-20s^4+160s^3t^3-45s^3t^2+60s^3t-15s^2t^3-10s^2t+20s^2+20st^3]$.

(7) $PI(G) = \frac{4}{3}\rho_{\mathrm{xy}}^2[(32s^2+32t^2)r^3+(8s^3+3072s^2t^2-750s^2t+54s^2-726st^2+54st-8s+54t^2)r^2+(8s^3+768s^2t^2-114s^2t-32s^2-90st^2-8s-32t^2)r+(2s^3+48s^2t^2-9s^2t-3st^2-2s)]$.

(8) $S(G) = \frac{8}{15}\rho_{\mathrm{xy}}(\gamma_{\mathrm{x}}+\gamma_{\mathrm{y}})[(-256s^2+24s-256t^2+24t)r^5+(1280s^2t-300s^2+1280st^2-240st+15s-300t^2+15t)r^4+(960s^2t-70s^2+960st^2-120st-70t^2)r^3+(-256s^5+1280s^4t+5120s^3t^2-720s^3t+7680s^2t^3-1800s^2t^2-340s^2t+300s^2-720st^3-340st^2+240st+241s+300t^2-15t)r^2+(-96s^5+480s^4t+1920s^3t^2-180s^3t+2880s^2t^3-450s^2t^2-675s^2t+326s^2-180st^3-675st^2+120st+72s+326t^2-24t)r+(-8s^5+40s^4t+160s^3t^2+240s^2t^3-100s^2t-100st^2+8s)]$.

(9) $Gut(G) = \frac{4}{15}\rho_{\mathrm{xy}}^2[(-2048s^2+384s-2048t^2+384t-36)r^5+(10240s^2t-2240s^2+10240st^2-3840st+300s-224t^2+300t)r^4+(5120s^2t-310s^2+5120st^2-960st-310t^2)r^3+(-2048s^5+10240s^4t+40960s^3t^2-11520s^3t+540s^3+61440s^2t^3-28800s^2t^2+400s^2t+2105s^2-11520st^3+400st^2+3300st+1613s+540t^3+2105t^2-435t)r^2+(-512s^5+2560s^4t+10240s^3t^2-1440s^3t+15360s^2t^3-3600s^2t^2-3480s^2t+2358s^2-1440st^3-3480st^2+960st+128s+2358t^2-384t+36)r+(-32s^5+160s^4t+640s^3t^2+960s^2t^3-400s^2t-400st^2+32s)]$.

(10) $Mo(G) = \frac{1}{3}\rho_{\mathrm{xy}}(\gamma_{\mathrm{x}}+\gamma_{\mathrm{y}})[(-32s^2-32t^2)r^3+(1536s^2t^2-288s^2t-288s^2-192t^2-288st^2-192(-1)^{r+s}t^2-192(-1)^{r+t}s^2-96(-1)^{s+t}s^2)r^2+(24(-1)^st^2-72st^2-72s^2t-112s^2-40t^2+24(-1)^ts^2+576s^2t^2-48(-1)^{r+s}t^2-48(-1)^{r+t}s^2-72(-1)^{s+t}s^2)r+(6(-1)^st^2-18s^2-6t^2+6(-1)^ts^2+48s^2t^2-12(-1)^{s+t}s^2)]$.

(11) $Mo_e(G) = \frac{1}{6}\rho_{\mathrm{xy}}^2[(-320s^2-320t^2)r^3+(264s+144t+432st-2952st^2-2808s^2t-2304s^2-48s^3-1536t^2+12288s^2t^2+144(-1)^{r+s}t+144(-1)^{r+t}s+72(-1)^{s+t}s-1536(-1)^{r+s}t^2-1536(-1)^{r+t}s^2-768(-1)^{s+t}s^2)r^2+(78s+18t-18(-1)^st-18(-1)^ts-396st^2-324s^2t-544s^2-24s^3-64t^2+192(-1)^st^2+192(-1)^ts^2+3072s^2t^2+36(-1)^{s+t}s-192(-1)^{r+s}t^2-192(-1)^{r+t}s^2-480(-1)^{s+t}s^2)r+(24(-1)^st^2-24t^2-72s^2+24(-1)^ts^2+192s^2t^2-48(-1)^{s+t}s^2)]$.

(12) $w^+Mo(G) = \frac{2}{3}\rho_{\mathrm{xy}}(\gamma_{\mathrm{x}}+\gamma_{\mathrm{y}})[(-96s^2+16s-96t^2+16t)r^3+(152s+144t-48(-1)^st-48(-1)^ts-1680st^2-1728s^2t-840s^2+16s^3-552t^2+6144s^2t^2+96(-1)^{r+s}t+96(-1)^{r+t}s+24(-1)^{s+t}s-768(-1)^{r+s}t^2-768(-1)^{r+t}s^2-384(-1)^{s+t}s^2)r^2+(22s+20t-12(-1)^st-12(-1)^ts-420st^2-432s^2t-216s^2+4s^3-48t^2+48(-1)^st^2+48(-1)^ts^2+1728s^2t^2+24(-1)^{r+s}t+24(-1)^{r+t}s+6(-1)^{s+t}s-144(-1)^{r+s}t^2-144(-1)^{r+t}s^2-192(-1)^{s+t}s^2)r+(12(-1)^st^2-24t^2-48s^2+12(-1)^ts^2+48s^2t^2+12(-1)^{r+s}t^2+12(-1)^{r+t}s^2-24(-1)^{s+t}s^2)]$.

(13) $w^+Mo_e(G) = \frac{1}{3}\rho_{\mathrm{xy}}^2[(-1024s^2+136s-1024t^2+136t)r^3+(1984s+1584t+2088st-384(-1)^st-384(-1)^ts-16032st^2-15840s^2t+36(-1)^s-6420s^2-64s^3+36(-1)^t-4116t^2-72(-1)^{r+s}-72*(-1)^{r+t}-18*(-1)^{s+t}+49152s^2t^2+1344(-1)^{r+s}t+1344(-1)^{r+t}s+480(-1)^{s+t}s-6144(-1)^{r+s}t^2-$

$6144(-1)^{r+t}s^2-3072(-1)^{s+t}s^2-198)r^2+(136s+8t-84(-1)^st-84(-1)^ts-1824st^2-1728s^2t-752s^2-32s^3+304t^2+384(-1)^st^2+384(-1)^ts^2+7680s^2t^2+60(-1)^{r+s}t+60(-1)^{r+t}s+96(-1)^{s+t}s-384(-1)^{r+s}t^2-384(-1)^{r+t}s^2-1152(-1)^{s+t}s^2)r+(48(-1)^st^2-96t^2-192s^2+48(-1)^ts^2+192s^2t^2+48(-1)^{r+s}t^2+48(-1)^{r+t}s^2-96(-1)^{s+t}s^2)]$.

(14) $w^*Mo(G)=\frac{2}{3}\rho_{\rm xy}^2(\gamma_{\rm x}+\gamma_{\rm y})[(-128s^2+56s-128t^2+56t)r^3+(536s+504t+96st-168(-1)^st-168(-1)^ts-4272st^2-4464s^2t-1344s^2+64s^3-864t^2+12288s^2t^2+336(-1)^{r+s}t+336(-1)^{r+t}s+96(-1)^{s+t}s-1536(-1)^{r+s}t^2-1536(-1)^{r+t}s^2-768(-1)^{s+t}s^2)r^2+(78s+70t+24st-42(-1)^st-42(-1)^ts-876st^2-924s^2t-112s^2+16s^3+56t^2+24(-1)^st^2+24(-1)^ts^2+2496s^2t^2+84(-1)^{r+s}t+84(-1)^{r+t}s+24(-1)^{s+t}s-192(-1)^{r+s}t^2-192(-1)^{r+t}s^2-240(-1)^{s+t}s^2)r+(48st^2+48s^2t-66s^2-54t^2+6(-1)^st^2+6(-1)^ts^2-144s^2t^2+48(-1)^{r+s}t^2+48(-1)^{r+t}s^2-12(-1)^{s+t}s^2)]$.

(15) $w^*Mo_e(G)=\frac{1}{3}\rho_{\rm xy}^3[(-1536s^2+464s-1536t^2+464t)r^3+(5464s+4680t+5664st-1344(-1)^st-1344(-1)^ts-39360st^2-39744s^2t+126(-1)^s-9660s^2+128s^3+126(-1)^t-5820t^2-252(-1)^{r+s}-252(-1)^{r+t}-72(-1)^{s+t}+98304s^2t^2+3840(-1)^{r+s}t+3840(-1)^{r+t}s+1344(-1)^{s+t}s-12288(-1)^{r+s}t^2-12288(-1)^{r+t}s^2-6144(-1)^{s+t}s^2-684)r^2+(6s-86t-192st-186(-1)^st-186(-1)^ts-2556st^2-2676s^2t+480s^2+40s^3+1344t^2+192(-1)^st^2+192(-1)^ts^2+7680s^2t^2+192(-1)^{r+s}t+192(-1)^{r+t}s+132(-1)^{s+t}s-1152(-1)^{s+t}s^2)r+(192st^2+192s^2t-264s^2-216t^2+24(-1)^st^2+24(-1)^ts^2-576s^2t^2+192(-1)^{r+s}t^2+192(-1)^{r+t}s^2-48(-1)^{s+t}s^2)]$.

(16) $w^+Sz(G)=\frac{16}{15}\rho_{\rm xy}(\gamma_{\rm x}+\gamma_{\rm y})^2[(-224s^3+3s^2-224t^3+32t^2)r^5+(480s^3t-840s^3-80s^2t+170s^2+480st^3-80st^2-840t^3+170t^2)r^4+(16s^5-80s^4t-400s^4+20480s^3t^3-960s^3t^2+1440s^3t+250s^3-1120s^2t^3-500s^2t+640s^2+640st^3-500st^2-16s+250t^3)r^3+(8s^5-40s^4t-360s^4+10880s^3t^3-480s^3t^2+530s^3t+1350s^3-560s^2t^3-160s^2t+310s^2-190st^3-160st^2-8s+1350t^3-170t^2)r^2+(s^5-5s^4t-105s^4+1600s^3t^3-60s^3t^2+250s^3t+214s^3-70s^2t^3-10s^2t+88s^2+40st^3-10st^2-s+214t^3-32t^2)r+(-10s^4+40s^3t^3+50s^3t+10s^2+30st^3)]$.

(17) $w^+Sz_e(G)=\frac{4}{15}\rho_{\rm xy}^3[(-15360s^3+3424s^2-186s-15360t^3+3424t^2-186t)r^5+(81920s^3t-60560s^3-18240s^2t+21080s^2+81920st^3-18240st^2+1980st-2370s-60560t^3+21080t^2-2370t+180)r^4+(-512s^5+12800s^4t-27040s^4+1310720s^3t^3-599040s^3t^2+226960s^3t+21220s^3-563200s^2t^3+155040s^2t^2-76690s^2t+38080s^2+172880st^3-53910st^2+12960st-7188s+16400t^3-4080t^2)r^3+(-320s^5+10560s^4t-17960s^4+368640s^3t^3-126720s^3t^2-10350s^3t+92830s^3-96640s^2t^3+20040s^2t^2-7670s^2t-5190s^2-46270st^3+7710st^2+330st+60s+90290t^3-26840t^2+2640t-180)r^2+(-32s^5+2400s^4t-3320s^4+30720s^3t^3-12240s^3t^2+3100s^3t-225s^3-5200s^2t^3+1320s^2t^2-2405s^2t+3481s^2-3540st^3+450st^2+120st-207s-470t^3-64t^2+6t)r+(160s^4t-190s^4+640s^3t^3-720s^3t^2+890s^3t-240s^2t^3-160s^2t+190s^2+510st^3)]$.

(18) $w^{+}PI(G) = \frac{8}{3}\rho_{xy}^{2}[(128s^2-16s+128t^2-16t)r^3+(32s^3+12288s^2t^2-3864s^2t+297s^2-3768st^2+516st-26s+297t^2)r^2+(24s^3+1920s^2t^2-390s^2t-104s^2-318st^2+15st-5s-104t^2+16t)r+(4s^3+48s^2t^2-18s^2t-6st^2-4s)]$.

(19) $w^{*}Sz(G) = \frac{16}{15}\rho_{xy}^{2}(\gamma_x+\gamma_y)^2[(-384s^3+112s^2-384t^3+112t^2)r^5+(640s^3t-1120s^3-280s^2t+595s^2+640st^3-280st^2-1120t^3+595t^2)r^4+(64s^5-320s^4t-560s^4+40960s^3t^3-3360s^3t^2+1120s^3t+760s^3-4000s^2t^3-1750s^2t+1280s^2-1750st^2-64s+760t^3)r^3+(32s^5-160s^4t-360s^4+18560s^3t^3-1680s^3t^2-440s^3t+2650s^3-2000s^2t^3-560s^2t+125s^2-1160st^3-560st^2-32s+2650t^3-595t^2)r^2+(4s^5-20s^4t-75s^4+1600s^3t^3-210s^3t^2+210s^3t+344s^3-250s^2t^3-35s^2t+8s^2+60st^3-35st^2-4s+344t^3-112t^2)r+(-5s^4-120s^3t^3+95s^3t+5s^2+85st^3)]$.

(20) $w^{*}Sz_e(G) = \frac{4}{15}\rho_{xy}^{4}[(-26624s^3+9344s^2-642s-26624t^3+9344t^2-642t)r^5+(143360s^3t-85920s^3-49920s^2t+53515s^2+143360st^3-49920st^2+6840st-7350s-85920t^3+53515t^2-7350t+630)r^4+(1024s^5+15360s^4t-38720s^4+2621440s^3t^3-1290240s^3t^2+372640s^3t+47230s^3-1239040s^2t^3+434880s^2t^2-191030s^2t+72320s^2+295200st^3-155910st^2+39480st-16419s+40430t^3-11760t^2+45t)r^3+(448s^5+11840s^4t-16180s^4+532480s^3t^3-190080s^3t^2-81510s^3t+176990s^3-152320s^2t^3+52380s^2t^2+7130s^2t-43545s^2-113870st^3+23250st^2-1920st+4752s+175110t^3-70795t^2+8160t-630)r^2+(40s^5+1880s^4t-2200s^4+10240s^3t^3-6480s^3t^2-1220s^3t-5836s^3-640s^2t^3+2520s^2t^2+35s^2t+3131s^2-5620st^3+2175st^2+60st-168s-5976t^3+256t^2+12t)r+(80s^4t-95s^4-1920s^3t^3-360s^3t^2+1565s^3t-120s^2t^3-80s^2t+95s^2+1375st^3)]$.

(21) $w^{*}PI(G) = \frac{8}{3}\rho_{xy}^{3}[(256s^2-56s+256t^2-56t)r^3+(64s^3+24576s^2t^2-9168s^2t+729s^2-8976st^2+1608st-55s+729t^2-9t)r^2+(36s^3+1920s^2t^2-477s^2t-202s^2-369st^2+30st+29s-202t^2+56t)r+(2s^3-144s^2t^2+15s^2t+21st^2-2s)]$.

Proof. In all three views, the Θ-classes of cuboid zeolite SAS materials are classified similarly to front-type rectangular SAS materials. Let $\{FFV_i^{rs}, FBV_i^{rs} : 1 \le i \le r+s-1\}$, $\{FVV_i^{rs} : 1 \le i \le t\}$ and $\{FHV_i^{rs} : 1 \le i \le t-1\}$ be the F-type classes in which FHV_i^{rs} stands for classes containing double 6-rings from front to back and all other classes have the same description of rectangular SAS. In the same way, we have S-type classes as $\{SFV_i^{rt}, SBV_i^{rt} : 1 \le i \le r+t-1\}$, $\{SVV_i^{rt} : 1 \le i \le s\}$ and $\{SHV_i^{rt} : 1 \le i \le s-1\}$. By the structural symmetry of SAS, the topological parameters are obtained for F-type class, say $f(r,s,t)$, then the corresponding S-type class is $f(r,t,s)$. Hence, if $\psi(r,s,t) = \sum_{i=1}^{r+s-1}\Big[\psi(FFV_i^{rs})+\psi(FBV_i^{rs})\Big] + \sum_{i=1}^{t}\psi(FVV_i^{rs}) + \sum_{i=1}^{t-1}\psi(FHV_i^{rs})$, then $\psi(r,t,s) = \sum_{i=1}^{r+t-1}\Big[\psi(SFV_i^{rt})+\psi(SBV_i^{rt})\Big] + \sum_{i=1}^{s}\psi(SVV_i^{rt}) + \sum_{i=1}^{s-1}\psi(SHV_i^{rt})$, where ψ is the topological index function. Finally, for T-type we have the classes as $\{TFV_i^{st}, TBV_i^{st} : 1 \le i \le t+s-1\}$.

The topological parameters of F-type classes are derived in the following.

$$\left|FFV_i^{rt}\right| = \begin{cases} 8ti\rho_{\mathrm{xy}} & : 1 \le i \le r-1 \\ 8rt\rho_{\mathrm{xy}} & : r \le i \le s \\ \left|FBV_{r+s-i}^{rs}\right| & : s+1 \le i \le r+s-1 \end{cases}$$

$$|FVV_i| = 2s(3r+1)\rho_{\mathrm{xy}}, \quad 1 \le i \le t$$
$$|FHV_i| = 6rs\rho_{\mathrm{xy}}, \quad 1 \le i \le t-1$$

$$w^+\left(FFV_i^{rs}\right) = \begin{cases} (8i(8t-1)-4t)\rho_{\mathrm{xy}} & : 1 \le i \le r-1 \\ (8r(8t-1)-8t)\rho_{\mathrm{xy}} & : i = r,\ r = s \\ (8r(8t-1)-6t)\rho_{\mathrm{xy}} & : i = r,\ r < s \\ (8r(8t-1)-4t)\rho_{\mathrm{xy}} & : r < i < s \\ w^+\left(FBV_{r+s-i}^{rs}\right) & : s \le i \le r+s-1 \end{cases}$$

$$w^*\left(FFV_i^{rs}\right) = \begin{cases} (4i(32t-7)-16t)\rho_{\mathrm{xy}}^2 & : 1 \le i \le r-1 \\ (4r(32t-7)-28t)\rho_{\mathrm{xy}}^2 & : i = r,\ r = s \\ (4r(32t-7)-22t)\rho_{\mathrm{xy}}^2 & : i = r,\ r < s \\ (4r(32t-7)-16t)\rho_{\mathrm{xy}}^2 & : r < i < s \\ w^*\left(FBV_{r+s-i}^{rs}\right) & : s \le i \le r+s-1 \end{cases}$$

$$w^+\left(FVV_i\right) = 8(6rs-(r-s))\rho_{\mathrm{xy}}, \quad 1 \le i \le t$$
$$w^*\left(FVV_i\right) = 4(24rs-(7r-s))\rho_{\mathrm{xy}}^2, \quad 1 \le i \le t$$

$$w^+\left(FHV_i\right) = 48rs\rho_{\mathrm{xy}}, \quad 1 \le i \le t-1$$
$$w^*\left(FHV_i\right) = 96rs\rho_{\mathrm{xy}}^2, \quad 1 \le i \le t-1$$

$$n\left(FFV_i^{rs}\right) = \begin{cases} 2t(4i+1)i(\gamma_{\mathrm{x}}+\gamma_{\mathrm{y}}) & : 1 \le i \le r-1 \\ 2t(2i(4r+1)-r(4r+1))(\gamma_{\mathrm{x}}+\gamma_{\mathrm{y}}) & : r \le i \le s \\ n\left(FBV_{r+s-i}^{rs}\right) & : r+1 \le i \le r+s-1 \end{cases}$$

$$m\left(FFV_i^{rs}\right)=\begin{cases}i((32t-3)i-3t)\rho_{\mathrm{xy}} & :\ 1\le i\le r-1\\ (2(32rt+4t-3r)i-r(32rt+11t-3r))\rho_{\mathrm{xy}} & :\ r\le i\le s\\ m\left(FBV_{r+s-i}^{rs}\right) & :\ s+1\le i\le r+s-1\end{cases}$$

$$n\left(FVV_i\right)=2s(4r+1)(2i-1)(\gamma_{\mathrm{x}}+\gamma_{\mathrm{y}}),\ \ 1\le i\le t$$
$$m\left(FVV_i\right)=(2i(32rs-3r+4s)-(38rs-3r+5s))\rho_{\mathrm{xy}},\ \ 1\le i\le t$$

$$n\left(FHV_i\right)=4s(4r+1)i(\gamma_{\mathrm{x}}+\gamma_{\mathrm{y}}),\ \ 1\le i\le t-1$$
$$m\left(FHV_i\right)=2((32rs-3r+4s)i-3rs)\rho_{\mathrm{xy}},\ \ 1\le i\le t-1$$

The topological parameters of T-type classes are presented in the following.

$$\left|TFV_i^{st}\right|=\begin{cases}(4r+2)i\rho_{\mathrm{xy}} & \text{if } 1\le i\le s-1\\ (4r+2)s\rho_{\mathrm{xy}} & \text{if } s\le i\le t\\ \left|TBV_{t+s-i}^{ts}\right| & \text{if } t+1\le i\le t+s-1\end{cases}$$

$$w^{+}\left(TFV_i^{st}\right)=\begin{cases}(8i(4r+1)-2r)\rho_{\mathrm{xy}} & :\ 1\le i\le s-1\\ (8s(4r+1)-4r)\rho_{\mathrm{xy}} & :\ i=s,\ s=t\\ (8s(4r+1)-3r)\rho_{\mathrm{xy}} & :\ i=s,\ s<t\\ (8s(4r+1)-2r)\rho_{\mathrm{xy}} & :\ s<i<t\\ w^{+}\left(TBV_{t+s-i}^{ts}\right) & :\ t\le i\le t+s-1\end{cases}$$

$$w^{*}\left(TFV_i^{st}\right)=\begin{cases}(4i(16r+1)-8r)\rho_{\mathrm{xy}}^2 & :\ 1\le i\le s-1\\ (4s(16r+1)-14r)\rho_{\mathrm{xy}}^2 & :\ i=s,\ s=t\\ (4s(16r+1)-11r)\rho_{\mathrm{xy}}^2 & :\ i=s,\ s<t\\ (4s(16r+1)-8r)\rho_{\mathrm{xy}}^2 & :\ s<i<t\\ w^{*}\left(TBV_{t+s-i}^{ts}\right) & :\ t\le i\le t+s-1\end{cases}$$

$$n\left(TFV_i^{st}\right)=\begin{cases}2i^2(4r+1)(\gamma_{\mathrm{x}}+\gamma_{\mathrm{y}}) & :\ 1\le i\le s-1\\ 2s(8ri-4sr+2i-s)(\gamma_{\mathrm{x}}+\gamma_{\mathrm{y}}) & :\ s\le i\le t\\ n\left(TBV_{t+s-i}^{ts}\right) & :\ t+1\le i\le s+t-1\end{cases}$$

$$m\left(TFV_i^{ts}\right) = \begin{cases} i(4(8r+1)i - 8r - 1)\rho_{\text{xy}} & : 1 \le i \le s-1 \\ (2i(32rs + 4s - 3r) - 4s^2(8r+1) - s(2r+1))\rho_{\text{xy}} & : s \le i \le t \\ m\left(TBV_{t+s-i}^{ts}\right) & : t+1 \le i \le t+s-1 \end{cases}$$

Hence, $\psi(SAS(r,s,t)) = \psi(r,s,t) + \psi(r,t,s) + 4\sum_{i=1}^{s-1} TI(TFV_i^{st}) + 2\sum_{i=s}^{t} TI(TBV_i^{st})$. □

3.1 Degree-based Topological Indices

The goal of the section is to compute the degree-based topological indices of zeolite SAS which depend on the edge partition of $SAS(r,s,t)$. Moreover, zeolite SAS materials have only x−y bond types, we consider the SAS materials with unit weight for each atom and bond. We notice that SAS has bonds with terminal degrees as 3−3, 3−4 and 4−4. Hence, the bond partition $D(SAS(r,s,t))$ based on the degrees is given below.

$\left|D_{33}\right| = 4[(3rs + 4st + 3tr) + (r + 2s + 2t)]$,

$\left|D_{34}\right| = 4[(3rs + 4st + 3tr) - 2(r + 2s + 2t)]$,

$\left|D_{44}\right| = 2[32rst - (15rs + 12st + 15tr) + 2(r + 2s + 2t)]$.

We can readily compute the degree-based topological quantities of SAS materials in light of the above edge partition by simple calculations given below.

Theorem 3.3. *For $r,s,t \ge 1$, let $G = SAS(r,s,t)$.*

(1) $M_1(G) = 4[128rst - (21rs - 4st + 21tr)]$.

(2) $M_2(G) = 4[256rst - (57rs + 12st + 57tr) + (r + 2s + 2t)]$.

(3) $R(G) = \frac{1}{6}[96rst - 3(7rs + 2st + 7tr) + 4\sqrt{3}(3rs + 4st + 3tr) + (14 - 8\sqrt{3})(r + 2s + 2t)]$.

(4) $ABC(G) = \frac{1}{6}[96\sqrt{6}rst + (4\sqrt{15} + 16)(3rs + 4st + 3tr) - 9\sqrt{6}(5rs + 4st + 5tr) + (6\sqrt{6} - 8\sqrt{15} + 16)(r + 2s + 2t)]$.

(5) $H(G) = \frac{1}{42}[672rst - (3rs - 164st + 3tr) + 2(r + 2s + 2t)]$.

(6) $HM(G) = 4[1024rst - (225rs + 44st + 225tr) + 2(r + 2s + 2t)]$.

(7) $SC(G) = \frac{1}{84}[1344\sqrt{2}rst - 126\sqrt{2}(5rs + 4st + 5tr) + (56\sqrt{6} + 48\sqrt{7})(3rs + 4st + 3tr) + (84\sqrt{2} + 56\sqrt{6} - 96\sqrt{7})(r + 2s + 2t)]$.

(8) $GA(G) = \frac{1}{7}[448rst - 14(9rs + 4st + 9tr) + 16\sqrt{3}(3rs + 4st + 3tr) + (56 - 32\sqrt{3})(r + 2s + 2t)]$.

(9) $irr(G) = 4[(3rs + 4st + 3tr) - 2(r + 2s + 2t)]$.

(10) $F(G) = 4[512rst - (111rs + 20st + 111tr)]$.

(11) $SDD(G) = \frac{1}{3}[384rst - (33rs - 52st + 33tr) - 2(r + 2s + 2t)]$.

3.2 Numerical Computations

In this section, we present the numerical values of topological measures of cubic SAS materials by substituting the relativistic parameters as $\gamma_x = \gamma_y = \rho_{xy} = 1$ in Table 1 and the graphical representation in Figure 5. The numerical values for the topological indices were also cross validated with computations carried out using TopoChemie-2020 [38].

Table 1: Topological measures of cubic SAS zeolite of dimension r

Index	$r = 2$	$r = 3$	$r = 4$	$r = 5$	$r = 6$
irr	80	240	480	800	1200
H	143.52	466.57	1085.14	2095.24	3592.86
R	143.76	467.28	1086.56	2097.61	3596.41
SC	188.25	627.04	1476.62	2872.77	4951.23
ABC	317.25	1066.89	2524.08	4923.97	8501.70
GA	495.18	1689.54	4027.07	7891.79	13667.69
SDD	998.67	3404	8104	15866.67	27460
M_1	3488	12456	30336	60200	105120
M_2	6216	23172	57552	115500	203160
F	12512	46584	115584	231800	407520
HM	24944	92928	230688	462800	813840
M	51392	672192	3958528	15395200	46491840
Mo_e	91840	1246032	7476224	29406400	89479872
PI	234384	2778376	15906464	61347720	184509104
W	343744	5471872	39444352	183595904	647056448
w^+Mo	355712	4921920	29608448	116828800	355847040
W_{ev}	547072	9369208	70135168	334040264	1195634432
w^*Mo	619904	9080832	55762432	222995200	684589440
w^+Mo_e	635648	9124704	55924224	223169600	684910080

Index	$r = 2$	$r = 3$	$r = 4$	$r = 5$	$r = 6$
W_e	867140	16008438	124548296	607256866	2207996556
w^*Mo_e	1107776	16837248	105334016	426003200	1317723456
w^+PI	1648160	20451616	119667968	467457680	1417742624
S	2331136	39060544	289314304	1369341056	4881033728
w^*PI	2936704	38041064	227006656	896805640	2739860416
Gut	3948960	69674992	530356672	2552785184	9203637728
Sz	7853440	268360512	3378570752	24348017600	122886909312
Sz_{ev}	12535168	460880880	6022680576	44394423440	227485488768
Sz_e	19947912	790282572	10726108960	80895673980	420931526280
w^+Sz	55482112	1985527296	25532505088	186250098560	947448168192
w^*Sz	99556096	3716662848	48687512576	358871618240	1837780599552
w^+Sz_e	141072464	5849768256	81077530304	618888859960	3245596498320
w^*Sz_e	253453200	10955530164	154642470336	1192649352860	6296045739600

3.3 Computations of Spectra and Vertex Partitions and Their Applications to Spectroscopy

One of the most important applications of graph theoretical analysis of networks of zeolites is the ability to predict their graph spectra and the vertex partitions of the networks which in turn can be applied to machine learning of NMR spectra as well as ESR hyperfine structures of these zeolites. In this section we employ the distance degree based sequence vector (DDSV) technique to partition the vertices of these networks as an algorithm for the machine learning of spectral features of these networks. Moreover we also obtain the graph spectra of these networks and compare the graph spectral properties of $SAS(r, s)$ and $SAS(r, s, t)$.

We consider five zeolites namely, $SAS(2, 2)$, $SAS(2, 3)$, $SAS(3, 3)$, $SAS(2, 2, 2)$ and $SAS(3, 3, 3)$ to demonstrate the techniques. The vectorial distance degree sequence (DDSV) of a vertex v in a general graph G is defined as an integer sequence which is comprised of the number of vertices at distances $0, 1, 2, ..., e_v$, where e_v is the eccentricity of v in G [39]. The DDSV can be denoted by a p-tuple vector $(d_{i0}, d_{i1}, d_{i2}, ..., d_{ij}, ..., d_{ip})$ for each vertex v_i in the graph where d_{ij} is the number of vertices at distance j from the vertex v_i. The algorithm for computing the DDSV starts with the generation of graph distance matrix from the adjacency matrix. The DDSV is for each vertex is computed by using the computer code TopoChemie-2020 [38]. Two equivalent vertices under the graph automorphism would have the same DDSV although we note that the converse is not true. For the zeolite network

structures considered here, the DDSV technique offers a viable technique for the vertex partitioning. There are $|V|$ such DDSV vectors of variable lengths for a network containing $|V|$ vertices. As the DDSV vector is of variable length, we concatenate all the entries of a given DDSV into a single long integer label assigned to each vertex. The concatenation algorithm thus employed offers a simple and yet viable alternative to comparison of long integer labels of different vertices in order to arrive at the vertex partitions on the basis of the concatenated labels on the vertices. In addition we have also computed the graph spectra of the networks in order to compare them. Table 2 compares the vertex partitions and graph spectra of five SAS zeolites (three square and two cubic SAS zeolites).

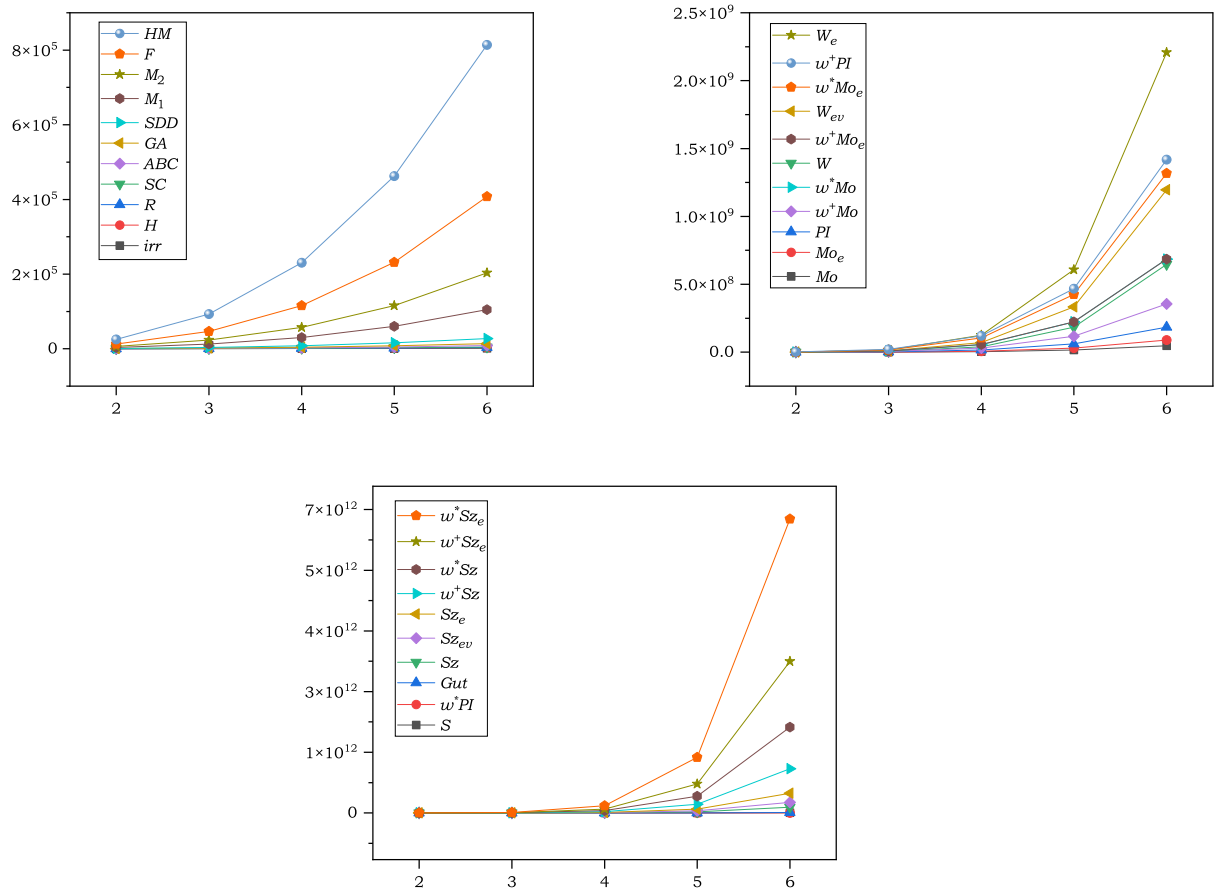

Figure 5: Graphical representation of topological values of cubic zeolite $SAS(r, r, r)$

As can be seen from Table 2, the vertices of three square SAS structures exhibit the partition 4^i8^j for some integers i and j. In particular the $SAS(2, 2)$, $SAS(2, 3)$ and $SAS(3, 3)$ structures exhibit 4^48^{16}, 4^68^{24} and 4^68^{36} vertex partitions, respectively. The vertex partitions have direct a bearing on the corresponding NMR spectra depending on the nuclei included in the partitions. Likewise a free radical generated from the zeolite would exhibit ESR hyperfine patterns arising from the coupling of

the unpaired electron with the nuclei in the partition closest to the unpaired electron. The cubic SAS structures exhibit different types of vertex partitions with 16-membered and 8-membered classes (Table 2). The $SAS(2,2,2)$ cubic structure exhibits the vertex partition $16^{16}8^4$ whereas the $SAS(3,3,3)$ cubic structure exhibits the $16^{54}8^9$ vertex partition.

Table 2: Vertex partitions and spectral properties of SAS zeolite

Zeolite Type	**Square**			**Cubic**	
	$SAS(2,2)$	$SAS(2,3)$	$SAS(3,3)$	$SAS(2,2,2)$	$SAS(3,3,3)$
$\|V\|$	144	216	312	288	936
$\|E\|$	236	360	528	496	1692
Vertex Partitions From DDSV	$4^4\ 8^{16}$	$4^6\ 8^{24}$	$4^6\ 8^{36}$	$16^{16}\ 8^4$	$16^{54}\ 8^9$
HOMO-LUMO	0.03355β	0.026866β	0.000068β	$0.183166\beta^*$	0.040416β
Spectral Diameter	7.303612β	7.34931β	7.445224β	7.54948β	7.789784β
Mirror Symmetry of Spectra	Yes	Yes	Yes	Yes	Yes
Bond Degrees 3−3	136	184	236	200	420
3−4	40	64	104	80	240
4−4	60	112	188	216	1032

*HOMO and LUMO are both doubly-degenerate

Figure 6 shows the ESR hyperfine structures arising from the interaction of the unpaired electron for the square and cubic SAS structures. For the square structure we have shown the machine-generated ESR hyperfine pattern arising from the interaction of an unpaired electron with two kinds of nuclear partitions, one containing two sets of 8 nuclei and the other containing an equivalence class of 4 nuclei that are nearest to the unpaired electron. Since the partitions containing 8 and 4 vertices seems to be common in the square SAS zeolites under consideration we have chosen these sets of equivalence classes which we call $8 \times 8 \times 4$ partition coupling. The result of such an ESR hyperfine structure for the SAS zeolites is shown in Figure 6a as a typical example. Likewise as the cubic SAS structures exhibit 16^i8^j partitions, we show in Figure 6b, machine-generated ESR hyperfine structure arising from the coupling of an unpaired electron with two sets of 16 nuclei and one set of 8 nuclei. It can be seen from Figure 6a and Figure 6b, the square and cubic structures exhibit contrasting hyperfine patters. The actual spectra would depend on the nuclear isotopes in the partition that are closest to the unpaired electron.

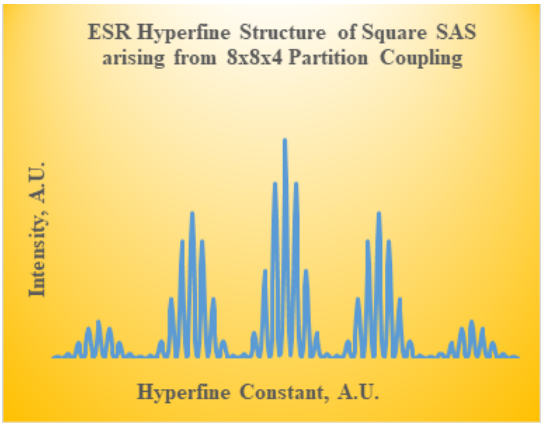

(a)

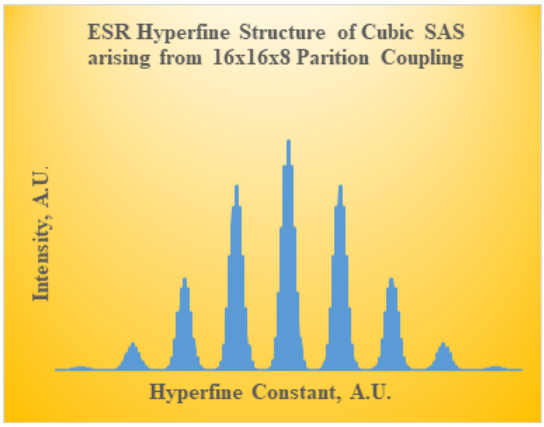

(b)

Figure 6: Computer-generated hyperfine structure for SAS zeolites (a) A square SAS with $8 \times 8 \times 4$ partition coupling (b) A cubic SAS with $16 \times 16 \times 8$ partition coupling

The graph spectra of the SAS zeolites are the eigenvalues of the corresponding characteristic polynomials of the network. The graph spectra of these networks get crowded due to a large number of vertices and owing to the fact that the maximal degrees of the vertices is 4. Thus even though we show the various spectral values in terms of the Hückel energy parameter β, these values should not be directly interpreted as energy values. A general trend that we see is that the gap between the largest negative eigenvalue and the smallest positive eigenvalue (HOMO-LUMO gap) decreases as the network size increases due to the crowding of graph spectra as the size of the network increases. The spectral diameter which is defined as the difference between the lowest and highest eigenvalues increases as a function of the zeolite size. The diameter must be confined to two times the maximal vertex degree, and thus the spectral crowding arises from this constraint. All the SAS structures considered here exhibit spectral mirror symmetry as these are bipartite graphs and thus spectral pairing occurs in that for each eigenvalue λ_i there exists an eigenvalue $-\lambda_i$ in the graph network spectra. In comparing the cubic structures with the square structures, we note that there are several doubly-degenerate eigenvalues for the cubic structures whereas for the square structures the eigenvalues do not exhibit any degeneracy. For the $SAS(2,2,2)$, the HOMO and LUMO are both doubly-degenerate while this is not the case for the $SAS(3,3,3)$ cubic structure suggesting the possibility of an odd-even alternation relative to the degeneracy of the HOMOs and LUMOs for the cubic structures.

4 Conclusion

In this paper, we have studied the graph theoretical framework topology of zeolite SAS networks by incorporating the relativistic quantum parameters through weighted chemical graphs of the networks. As the investigation of such complex SAS networks can be a daunting task, we have employed an elegant graph theoretical cut methods to derive various topological indices of these networks. Such techniques would have potential future applications in computing physicochemical properties of large SAS zeolites containing very heavy atoms and thus could find applications in the fields of catalysis, gas separation, and environmental remediation. This study will also give new impetus for the potential synthesis of new isomorphic zeotypes of industrial, medical and environmental importance. Graph-theoretically implemented algorithms could pave the way for machine learning and artificial intelligence applications to structures and spectroscopy of these cages including analysis of various channels and pathways for transport of materials through porous media.

References

[1] M. Krol, Natural vs synthetic zeolites, Crystals **10**(7) (2020) 622.

[2] J.M. Newsam, The zeolite cage structure, Science **231** (1986) 1093–1099.

[3] A. Primo, H. Garcia, Zeolites as catalysts in oil refining, Chem. Soc. Rev. **43**(22) (2014) 7548–7561.

[4] R.M. Franco, A. Cantin, M. Moliner, A. Corma, Synthesis of the small pore silicoaluminophosphate STA 6 by using supramolecular self–assembled organic structure directing agents, Chem. Mater. **26** (2014) 4346–4353.

[5] M. Moliner, C. Martinez, A. Corma, Synthesis strategies for preparing useful small pore zeolites and zeotypes for gas separation and catalysis, Chem. Mater. **26**(1) (2014) 246–258.

[6] P.Vinaches, K.B. Gusmao, S.B.C. Pergher, An introduction to zeolite synthesis using imidazolium-based cations as organic structure directing agents, Molecules **22**(8) (2017) 1307.

[7] M. Dusselier, M.E. Davis, Small-pore zeolites: synthesis and catalysis, Chem. Rev. **118**(11) (2018) 5265–5329.

[8] C.Y. Chen, S.I. Zones, Investigation of small-pore zeolites via vapor phase adsorption of n-hexane, Chem. Ing. Tech. **93**(6) (2021) 959–966.

[9] D.S. Wragg, R. Morris, A.W. Burton, S.I. Zones, K. Ong, G. Lee, The synthesis and structure of SSZ-73: An all-silica zeolite with an unusual framework topology, Chem. Mater. **19** (2007) 3924–3932.

[10] A.M. Elhassan, Study of the physical properties of sudan natural and synthetic zeolites modification by PT element, Int. J. Adv. Res. **4**(9) (2016) 1692–1711.

[11] M. Zaarour, B. Dong, I. Naydenova, R. Retoux, S. Mintova, Progress in zeolite synthesis promotes advanced applications, Microporous Mesoporous Mater. **189** (2014) 11–21.

[12] M.E. Davis, Ordered porous materials for emerging applications, Nature **417** (2002) 813-821.

[13] P.A. Wright, M.J. Maple, A.M.Z. Slawin, V. Patinec, R.A. Aitken, S. Welsh, P.A. Cox, Cation-directed syntheses of novel zeolite-like metalloaluminophosphates STA-6 and STA-7 in the presence of azamacrocycle templates, J. Chem. Soc. Dalton Trans. **8** (2000) 1243–1248.

[14] V. Patinec, P.A. Wright, P. Lightfoot, R.A. Aitken, P.A. Cox, Synthesis of a novel microporous magnesioaluminophosphate, STA-6, containing an unbound azamacrocycle, J. Chem. Soc. Dalton Trans. **22** (1999) 3909–3911.

[15] M Arockiaraj, J. Clement, D. Paul, K. Balasubramanian, Quantitative structural descriptors of sodalite materials, J. Mol. Struct. **122** (2020) 128766.

[16] M Arockiaraj, D. Paul, S. Klavžar, J. Clement, S. Tigga, K. Balasubramanian, Relativistic distance based and bond additive topological descriptors of zeolite RHO materials, J. Mol. Struct. **1250** (2021) 131798.

[17] M. Arockiaraj, J. Clement, D. Paul, K. Balasubramanian, Relativistic distance based topological descriptors of Linde type A zeolites and their doped structures with very heavy elements, Mol. Phys. **119**(3) (2021) e1798529.

[18] O. Ivanciuc, QSAR comparative study of Wiener descriptors for weighted molecular graphs, J. Chem. Inf. Comput. Sci. **40**(6) (2000) 1412–1422.

[19] N. De, M. Cancan, M. Alaeiyan, M.R. Farahani, On some degree based topological indices of mk-graph, J. Discret. Math. Sci. Cryptogr. **23**(6) (2020) 1183–1194.

[20] K. Balasubramanian, Relativistic Effects in Chemistry: Part A, Theory and Techniques and Relativistic Effects in Chemistry, John Wiley & Sons: New York, 1997.

[21] K. Balasubramanian, CASSCF/Cl calculations of electronic states and potential-energy surfaces of PtH_2, J. Chem. Phys. **87**(5) (1987) 2800–2805.

[22] K. Balasubramanian, K.K. Das, D.W. Liao, Spectroscopic Constants and Potential-Energy Curves for Hg_2, Chem. Phys. Lett. **195**(5-6) (1992) 487–493.

[23] K. Balasubramanian, CASSCF/CI calculations on Si_4 and Si_4^+, Chem. Phys. Lett. **135**(3) (1987) 283–287.

[24] S. Klavžar, I. Gutman, B. Mohar, Labeling of benzenoid systems which reflects the vertex-distance relation, J. Chem. Inf. Comput. Sci. **35**(3) (1995) 590–593.

[25] S. Klavžar, M.J. Nadjafi-Arani, Cut method: update on recent developments and equivalence of independent approaches, Curr. Org. Chem. **19** (2015) 348–358.

[26] S. Klavžar, M.J. Nadjafi-Arani, Wiener index in weighted graphs via unification of Θ^*-classes, European J. Combin. **36** (2014) 71–76.

[27] S. Brezovnik, N. Tratnik, General cut method for computing Szeged-like topological indices with applications to molecular graphs, Int. J. Quantum Chem. **121**(6) (2021) e26530.

[28] M. Arockiaraj, J. Clement, N. Tratnik, S. Mushtaq, K. Balasubramanian, Weighted Mostar indices as measures of molecular peripheral shapes with applications to graphene, graphyne and graphdiyne nanoribbons, SAR QSAR Environ. Res. **31**(3) (2020) 187–208.

[29] A. Ali, T. Došlić, Mostar index: Results and perspectives, Appl. Math. Comput. **404** (2021) 126245.

[30] E. Estrada, L. Torres, L. Rodríguez, I. Gutman, An atom-bond connectivity index: Modelling the enthalpy of formation of alkanes, Indian J. Chem. **37A**(10) (1998) 849–855.

[31] B. Furtula, I. Gutman, A forgotten topological index, J. Math. Chem. **53** (2015) 1184–1190.

[32] G.H. Shirdel, H. Rezapour, A.M. Sayadi, The hyper-Zagreb index of graph operations, Iranian J. Math. Chem. **4**(2) (2013) 213–220.

[33] S.R.J. Kavitha, J. Abraham, M. Arockiaraj, J. Jency, K. Balasubramanian, Topological characterization and graph entropies of tessellations of kekulene structures: Existence of isentropic structures and applications to thermochemistry, nuclear magnetic resonance, and electron spin resonance, J. Phys. Chem. A **125**(36) (2021) 8140–8158.

[34] E. Deutsch, S. Klavžar, M-polynomial and degree-based topological indices, Iranian J. Math. Chem. **6**(2) (2015) 93–102.

[35] G. Abbas, M. Ibrahim, A. Ahmad, M. Azeem, K. Elahi, M-polynomials of tetra-cyano-benzene transition metal structure, Polycyclic Aromatic Comp. (2022) DOI10.1080/10406638.2021.2019797.

[36] M. Kamran, N. Salamat, R.H. Khan, U.U.R. Asghar, M.A. Alam, M.K. Pandit, Computation of M-polynomial and topological indices of phenol formaldehyde, J. Chem. **2022** (2022) 8655347.

[37] S. Klavžar, S. Shpectorov, Tribes of cubic partial cubes, Discrete Math. Theor. Comput. Sci. **9** (2007) 273–292.

[38] K. Balasubramanian, Topochemie-2020-A Computational Package for Computing Topological Indices, Spectral Polynomials, Walks and Distance Degree Sequences and Combinatorial Generators, 2020.

[39] G.S. Bloom, J.W. Kennedy, L.V. Quintas, Some problems concerning distance and path degree sequences, In: M. Borowiecki, J.W. Kennedy, M.M. Sysło (eds), Graph Theory, Lecture Notes in Mathematics **1018** (1983) 179–190.